

Structural analysis of K^+ dependence in L-asparaginases from *Lotus japonicus*

Alfredo Credali · Antonio Díaz-Quintana ·
Margarita García-Calderón · Miguel A. De la Rosa ·
Antonio J. Márquez · José M. Vega

Received: 30 November 2010 / Accepted: 23 February 2011 / Published online: 10 March 2011
© Springer-Verlag 2011

Abstract The molecular features responsible for the existence in plants of K^+ -dependent asparaginases have been investigated. For this purpose, two different cDNAs were isolated in *Lotus japonicus*, encoding for K^+ -dependent (LjNSE1) or K^+ -independent (LjNSE2) asparaginases. Recombinant proteins encoded by these cDNAs have been purified and characterized. Both types of asparaginases are composed by two different subunits, α (20 kDa) and β (17 kDa), disposed as $(\alpha\beta)_2$ quaternary structure. Major differences were found in the catalytic efficiency of both enzymes, due to the fact that K^+ is able to increase by tenfold the enzyme activity and lowers the K_m for asparagine specifically in LjNSE1 but not in LjNSE2 isoform. Optimum LjNSE1 activity was found at 5–50 mM K^+ , with a K_m for K^+ of 0.25 mM. Na^+ and Rb^+ can, to some extent, substitute for K^+ on the activating effect of LjNSE1 more efficiently than Cs^+ and Li^+ does. In addition, K^+ is able to stabilize LjNSE1 against thermal inactivation. Protein homology modelling and molecular dynamics studies, complemented with site-directed mutagenesis, revealed the key importance of E248, D285 and E286 residues for the

catalytic activity and K^+ dependence of LjNSE1, as well as the crucial relevance of K^+ for the proper orientation of asparagine substrate within the enzyme molecule. On the other hand, LjNSE2 but not LjNSE1 showed β -aspartyl-hydrolase activity ($K_m = 0.54$ mM for β -Asp-His). These results are discussed in terms of the different physiological significance of these isoenzymes in plants.

Keywords Asparaginases · K^+ -Dependent enzyme activity · *Lotus* · Ntn-hydrolases · Nitrogen metabolism · Homology model

Abbreviations

BSA	Bovine serum albumin
ESP	Electrostatic surface potential
GOT	Glutamate-oxalacetate transaminase
IPTG	Isopropyl- β -D-thiogalactopyranoside
LjNSE1	Asparaginase 1 from <i>Lotus japonicus</i>
LjNSE2	Asparaginase 2 from <i>Lotus japonicus</i>
M^+	Monovalent cations
MD	Molecular dynamics
MDH	Malate dehydrogenase
NPT	Constant pressure and temperature
NVT	Constant volume and temperature
PME	Particle mesh Ewald method
RMSD	Root mean square deviation
RMSF	Root mean square fluctuations
XRD	X-ray diffraction

Electronic supplementary material The online version of this article (doi:10.1007/s00425-011-1393-0) contains supplementary material, which is available to authorized users.

A. Credali · M. García-Calderón · A. J. Márquez ·
J. M. Vega (✉)
Departamento de Bioquímica Vegetal y Biología Molecular,
Facultad de Química, Universidad de Sevilla, c/Prof. García
González, n° 1, Apartado 1203, 41071 Seville, Spain
e-mail: jmvega@us.es

A. Díaz-Quintana · M. A. De la Rosa
Instituto de Bioquímica Vegetal y Fotosíntesis, Centro de
Investigaciones Científicas, Isla de la Cartuja, c/Américo
Vespucio, s/n, 41092 Seville, Spain

Introduction

Asparagine has a N:C ratio of 2:4, which makes it an efficient molecule to store and transport reduced nitrogen

between plant tissues. In fact, asparagine is the major transport compound in the xylem from the root to the leaves and in the phloem from the leaves to the developing seeds in a range of plants (Lea et al. 2007). In *Lotus*, asparagine can account for 86% of the nitrogen flux from root to shoot, when the plant is adequately fed (Waterhouse et al. 1996). Work with this model legume has produced recently important methodological advances (Márquez 2005) and major breakthroughs in plant molecular biology, such as the identification of novel genes mainly involved in bacterial and mycorrhizal symbiosis (Udvardi et al. 2005; Stacey et al. 2006, and references therein). Nitrate and ammonium assimilation processes were previously studied in *L. japonicus* (Márquez et al. 2005). However, little is known yet on asparagine utilization in this plant.

L-Asparaginase (EC 3.5.1.1) catalyzes the hydrolysis of asparagine to aspartic acid and ammonium, which is subsequently reassimilated for other nitrogen compounds biosynthesis (Lea et al. 2007). Asparaginases can be divided into several families. The two best-characterized families include bacterial- and plant-type asparaginases, which are much less studied than the bacterial ones. Plant-type asparaginases, which comprise aspartyl-glucosaminidases (EC 3.5.1.26), involved in the catabolism of N-linked glycans (Borek and Jaskolski 2001; Borek et al. 2004) and plant asparaginases, belong to the superfamily of N-terminal nucleophile (Ntn-hydrolases). Plant asparaginases are evolutionary distinct from bacterial-type asparaginases but show about 66% sequence similarity to aspartyl-glucosaminidases, although their activity towards glycosylated asparagine was almost absent. Plant asparaginases are heterotetramers composed of two different subunits formed by auto-proteolytic cleavage of a single polypeptide precursor, exposing an N-terminal catalytic nucleophile (Borek et al. 2004).

The presence of both K⁺-dependent and K⁺-independent asparaginases in plants was reported in the literature (Sodek et al. 1980; Bruneau et al. 2006; Cañas et al. 2007). However, the exact significance of each of these isoenzymes is poorly understood (Lea et al. 2007), in spite of the fact that potassium is the most abundant inorganic cation in plants, comprising up to 10% of a plant's dry weight (Leigh and Wyn Jones 1984). The functions of potassium can be classified into those that rely on high and relatively stable concentrations of K⁺ in certain cellular compartments and those that depend on K⁺ mobility between different compartments, cells, or tissues. The first class function includes enzyme activation, stabilization of protein synthesis, and neutralization of protein negative charges (Marschner 1995).

The crystal structure of the K⁺-independent plant-type asparaginase from yellow lupine (*Lupinus luteus*) has been solved (Michalska et al. 2006). However, there are not

structural reports on the K⁺-dependent asparaginase isoform and the molecular features responsible for the K⁺-requirement of this enzyme.

In this paper, we compare at the molecular level K⁺-dependent and K⁺-independent asparaginase isoforms from *Lotus japonicus*. This work enabled us to investigate further the role of K⁺ in plant-type asparaginases and identify the crucial amino acid residues responsible for the interaction with K⁺.

Materials and methods

Plant materials and treatment

L. japonicus (Regel) Larsen ecotype B-129 Gifu was initially obtained from Prof. Jens Stougaard (University of Aarhus, Denmark) and then self-propagated at the University of Seville. Plant seeds were scarified and surface-sterilized, germinated in Agar/Horned Petri dishes, and transferred to pots using vermiculite as solid support. Five seedlings were placed in each pot and grown during 35 days in a chamber under 16/8 h day/night, 20/18°C, with a photosynthetic photon flux density of 250 μmol m⁻² s⁻¹ and a constant humidity of 70%. Plants were watered with Hornum nutrient solution (Handberg and Stougaard 1992).

Cloning of *L. japonicus* asparaginase cDNAs

For RNA extraction, leaf material was immediately frozen in liquid nitrogen, and then homogenized with a pestle over a mortar and kept at -80°C until use. The RNA was extracted using the RNeasy Plant Mini Kit and buffer RLT (Qiagen). Five micrograms of RNA was treated with RNase-free DNase (Ambion) according to the manufacturer's protocol. The Superscript III (Invitrogen) was used to synthesize cDNA from 1 μg of RNA. The LjNSE1 and LjNSE2 cDNA were amplified with Accuzyme DNA polymerase (Bioline, <http://www.bioline.com>) and the following primers: LjNSE1 (forward) 5'-CACCATGGGAAGGTGGGCAATC-3', (reverse) 5'-TTCCCATATTCCAACCTCC-3' and LjNSE2 (forward) 5'-CACC ATG GGT TGG GCA ATT GCT CT-3', (reverse) 5'-TCC CTC AAT TTT AGC AGC AGGC-3'.

These primers were designed to clone blunt-end PCR products into pET101/TOPO vector (Invitrogen) by transformation in *E. coli* XL1B (Agilent) and growth in Luria-Bertani (LB) medium containing 50 μg ml⁻¹ ampicillin. The inserts were verified by sequencing. The plasmids were then extracted by miniprep using Accuprep Plasmid Mini Extraction Kit (Bioneer, <http://www.bioneer.com>)

and transformed in *E. coli* BL21 Star (Invitrogen) grown in LB medium containing 50 µg ml⁻¹ ampicillin.

Site-directed mutagenesis of asparaginase cDNAs

The QuikChange IITM site-directed mutagenesis kit (Stratagene) was used according to the manufacturer’s instructions. The PCR-based mutagenesis protocol was performed using PET101/D-TOPO vectors harboring the respective asparaginase cDNAs. Mutant cDNAs were fully sequenced to ensure fidelity. Mutagenic primers are listed in Table 1.

Production and purification of recombinant proteins

The production of recombinant asparaginases in *E. coli* cultures (*A*₆₀₀=0.6) was induced with 1 mM isopropyl-β-D-thiogalactopyranoside (IPTG), and the cells were allowed to grow during 4 h at 37°C in the case of wild-type proteins and 24 h at 15°C in the case of the mutants. Then, they were centrifuged at 4,000g, at 4°C for 15 min, resuspended in 4 ml (per mg of pellet fresh weight) of standard buffer (50 mM Tris–HCl pH 8.0 containing 10 mM imidazole and 1 mM phenyl-methane-sulfonyl fluoride), and sonicated, at 0°C, by 3 cycles of 10 min, at 30 kHz power. The homogenate was centrifuged at 27,000g for 30 min at 4°C and the supernatant, once filtered through a 45 µm syringe filter membrane, was used as the crude extract.

As the C termini of recombinant asparaginases have a His-tag, the proteins were easily purified by affinity chromatography using a nickel-agarose gravity trap column (GE Healthcare) equilibrated with standard buffer. The standard purification procedure started with 5–10 g (fresh

weight) of cells, and the corresponding crude extract was passed through a column packed with 2 ml of Ni Sepharose 6 Fast Flow resin, which retained the recombinant proteins. The column was first washed with standard buffer, then with 50 mM Tris–HCl pH 8.0 buffer containing 50 mM imidazole, and, finally, recombinant asparaginase was eluted with the same buffer supplemented with 0.5 M imidazole. Purified proteins were dialyzed overnight against 50 mM Tris–HCl pH 8.0 buffer, at 4°C, and stored at –80°C in the same buffer containing 40% (v/v) glycerol. Final yield obtained were about 1 mg protein per liter of culture in the case of wild type and 0.3–0.5 mg for mutants. The electrophoretic homogeneity of protein preparations was confirmed by SDS-PAGE on 20% (w/v) acrylamide gels.

Protein was determined according to Bradford (1976) using bovine serum albumin (BSA) as standard.

Asparaginase enzyme activity measurements

The L-asparaginase assay measuring the release of L-Asp as a reaction product was performed according to Möllering (1985) based on subsequent transamination from aspartate to α-ketoglutarate, catalyzed by glutamate-oxalacetate transaminase (GOT) releasing oxalacetate, followed by malate dehydrogenase (MDH)-mediated reduction of oxalacetate to malate using NADH. The decrease in NADH concentration was measured, at 340 nm, using a Beckman DU 640 spectrophotometer. All the reagents and enzymes for the GOT and MDH coupled assay were obtained from Sigma. Each reaction was performed at room temperature in 1 ml of 20 mM Tris–HCl buffer, pH 7.5, containing 0.1 mM of α-ketoglutarate, 0.2 mM of NADH, 12.5 units each of GOT and MDH, as well as the corresponding asparaginase substrate, typically 50 mM L-Asn. The assay mixture was preincubated for about 10 min at room temperature until a plateau in absorbance at 340 nm was reached, thus allowing to register the small decrease of NADH concentration due to L-Asp impurities in the commercial L-Asn samples. Then, about 2.5–10 µg in 20 µl of Tris buffer of recombinant asparaginase per assay was added and absorbance at 340 nm continuously monitored, at 25°C. In the case of mutants with low activity, the recording time of absorbance at 340 nm was increased and the amount of recombinant enzyme used per assay was 50–100 µg. *K*_m values were calculated fitting initial velocity plots to Michaelis–Menten equation (*r*² ≥ 0.99). β-Asp-His hydrolase activity was determined using the same enzymatic assay procedure but replacing L-Asn for 5 mM β-Asp-His as substrate. For the calculation of *K*_m values substrate concentrations ranged between 1 and 75 mM in the case of Asn and 0.1–7.5 mM in the case of β-Asp-His.

Table 1 Primers used to introduce mutations into the cloned LjNSE1

Mutant	Primers (forward/reverse)
E248K	5'GGTGTCTCATGCACCGGAA <u>AAA</u> GGCGAGGC3' 5'GCCTCGCCTTTTCCGGTGCATGAGACACC3'
D285P	5'GCATCGTTTG <u>CCT</u> GAAAGGCTTGGCGGGCC3' 5'GGCCCCCAAGCCTTCAGGCAAACGATGC3'
E286K	5'GCATCGTTTGAT <u>AAA</u> GGCTTGGCGGGCC3' 5'GGCCCCCAAGCCTTTATCCAACGATCC3'
D285P-E286K	5'GCATCGTTTG <u>CCT</u> TAAAGGCTTGGCGGGCC3' 5'GGCCCCCAAGCCTTTAGGCAAACGATGC3'

Each mutation was introduced by the underlined nucleotides in the corresponding forward (upper) and reverse (lower) primers. Double mutant E248K-E286K and E248-D285P was produced by mutation of E248K single mutant using the same E286K or D285P single mutant primers. Triple mutant E248K-D285P-E286K was produced by mutation of E248K single mutant using D285P-E286K double mutant primers

Electrophoretic analysis

SDS-PAGE protein analysis was performed on gels containing 20% (w/v) acrylamide according to the procedure of Laemmli (1970). The proteins were stained in gels with Coomassie blue dye.

Analytical ultracentrifugation

Analytical ultracentrifugation was done in a Beckman Optima XL-A ultracentrifuge equipped with automatic system to follow protein migration. Sedimentation coefficient data were analyzed with the SVEDBERG program (Philo 1997). The sedimentation coefficients obtained were corrected for the temperature and the buffer composition using the program SEDNTERP (Laue et al. 1992) to calculate the sedimentation coefficient at 20°C and water ($s_{20,w}$).

MALDI-TOF mass spectrometry

The enzyme samples were mixed with an equal volume of a saturated sinapinic acid solution in 33% (v/v) acetonitrile solution containing 0.1% (w/v) trifluoroacetic acid. Mass spectra were registered in a Voyager Elite model spectrometer equipped with delayed extraction, according to Aitken (2005).

Sequence analysis

Multiple amino acid sequence alignments were performed with ClustalW (Thompson et al. 1994), using default parameters, and were manually adjusted in GeneDoc (<http://nrbsc.org/gfx/genedoc>).

Molecular modelling

Molecular modelling calculations were performed on the structure of K^+ -dependent asparaginase from *Lotus japonicus*, modelled from the X-ray structure of the plant K^+ -independent enzyme (Michalska et al. 2006), the *E. coli* enzyme precursor (Michalska et al. 2008) and the enzyme bound to L-aspartate (Michalska et al. 2005) as deposited at PDB (Berman et al. 2000) (access codes 2GEZ, 2ZAK and 2ZAL, respectively). Sequence identities of LjNSE1 with respect to the targets were 56, 40 and 52%, respectively. Models were built with Modeller 9v2 (Eswar et al. 2008). MD simulations were carried out using AMBER 9.0 (Case et al. 2006) under the AMBER 99 force field (Wang et al. 2000) in a Dell PowerEdge-based cluster. All calculations were run under periodic boundary conditions using an orthorhombic (minimum distance between protein and cell faces was initially set to 10 Å) cell geometry and PME

electrostatics with a Ewald summation cut off of 9 Å. Counter-ions were added and all systems were solvated with TIP3P water molecules (Jorgensen et al. 1983) (see Table S1 in Supplemental data), using the TLEAP module of AMBER. Protein side chains were then energy-minimized (250 steepest descent and 750 conjugate gradient steps) down to a RMS energy gradient of 0.01 $\text{kJ mol}^{-1} \text{Å}^{-1}$, using the SANDER module of AMBER. Afterwards, solvent and counter-ions were subjected to 500 steps of steepest descent minimization followed by 300 ps NPT-MD computations using isotropic molecule position scaling and a pressure relaxation time of 2 ps at 298 K. Temperature was regulated with Berendsen's heat bath algorithm (Berendsen et al. 1984), with a coupling time constant equal to 0.5 ps. After 100 ps simulation, the density of the system reached a plateau. Then, for each protein, the whole system was energy minimized and submitted to NVT-MD at 298 K, using 1.6 fs integration time steps. Snapshots were saved every 4 ps SHAKE algorithm (Ryckaert et al. 1977) was only used to constrain bonds involving hydrogen atoms. Cavity searches were carried out at the CASTp server (Dundas et al. 2006). Ligand docking was performed using UCSF Dock6 (Lang et al. 2009).

Coordinate files were processed using both the ptraj module of AMBER and the VMD (Humphrey et al. 1996) packages to perform alignments, RMSD calculations and secondary structure determination by the Kabsch and Sander (1983) algorithm. Data from the first 300 ps were considered as equilibration steps, and not included in any analysis. Electrostatic calculations were performed and represented in UCSF Chimera (Pettersen et al. 2004), using distance-dependent dielectrics.

Statistical analysis of the results

All enzyme assays were performed in triplicate. In all cases a linear correlation was observed between the amount of product formed and the length of time or amount of enzyme present in the assay. Error bar is \pm SD. Activity values in Fig. 9 have been analyzed with Student's *t* test ($P \leq 0.05$). Values of $+K^+/M^+$ activity ratio in Fig. S4 have been analyzed with one-way ANOVA ($P \leq 0.01$).

Results

cDNA cloning, recombinant expression and molecular properties of asparaginases from *Lotus japonicus*

Two genes coding for asparaginase isoenzymes, LjNSE1 (accession number, chr5.CM0096.20.nc) and LjNSE2 (accession number, LjT13A22.50.nc), were identified in

L. japonicus genome (<http://www.kazusa.jp>). The amino acid sequences deduced for LjNSE1 and 2 polypeptides are shown in Fig. 1. Both sequences lack a signal peptide (SignalP program, Nielsen et al. 1997; Bendsten et al. 2004), thus indicating the cytosolic location of the correspondingly expressed proteins. A high sequence identity was found between the different asparaginases from *L. japonicus* and *A. thaliana*. One of the sequences found (LjNSE1) showed a higher degree of amino acid identity (83%) with the K⁺-dependent asparaginase from *A. thaliana* (accession number, At3g16150). In contrast, LjNSE2 protein sequence showed a larger degree of amino acid identity (76%) with the K⁺-independent enzyme (accession number, At5g08100). LjNSE1 and 2 show ca. 60% of sequence identity.

Specific primers were designed to further PCR amplify and clone the LjNSE1 and LjNSE2 cDNAs, followed by heterologous expression in *E. coli* using pET101/TOPO

vectors. The presence of a C-terminal His-tag allowed the purification of recombinant asparaginases using a single step of metal-affinity chromatography. SDS-PAGE analysis indicated that each of the mature isoenzymes (LjNSE1 and LjNSE2) was composed by two types of subunits: α and β , with an apparent molecular weight of about 24.5 and 17 kDa, respectively (Fig. 2). Subunits α and β result from the auto-proteolytic cleavage of the corresponding polypeptide precursor encoded by each of LjNSE1 and LjNSE2 cDNAs. Mass spectrometric analysis of purified protein preparations revealed a molecular mass of 20.90 ± 0.15 kDa and 17.11 ± 0.15 kDa for α and β (including the His-tag) subunits of LjNSE1, respectively, and 20.18 ± 0.15 kDa and 17.33 ± 0.15 for the same in LjNSE2 (Fig. S1 in Supplemental data). These results are compatible with the existence of a single protein cleavage site placed at the peptide bond next to the expected highly conserved Thr residue previously reported to be

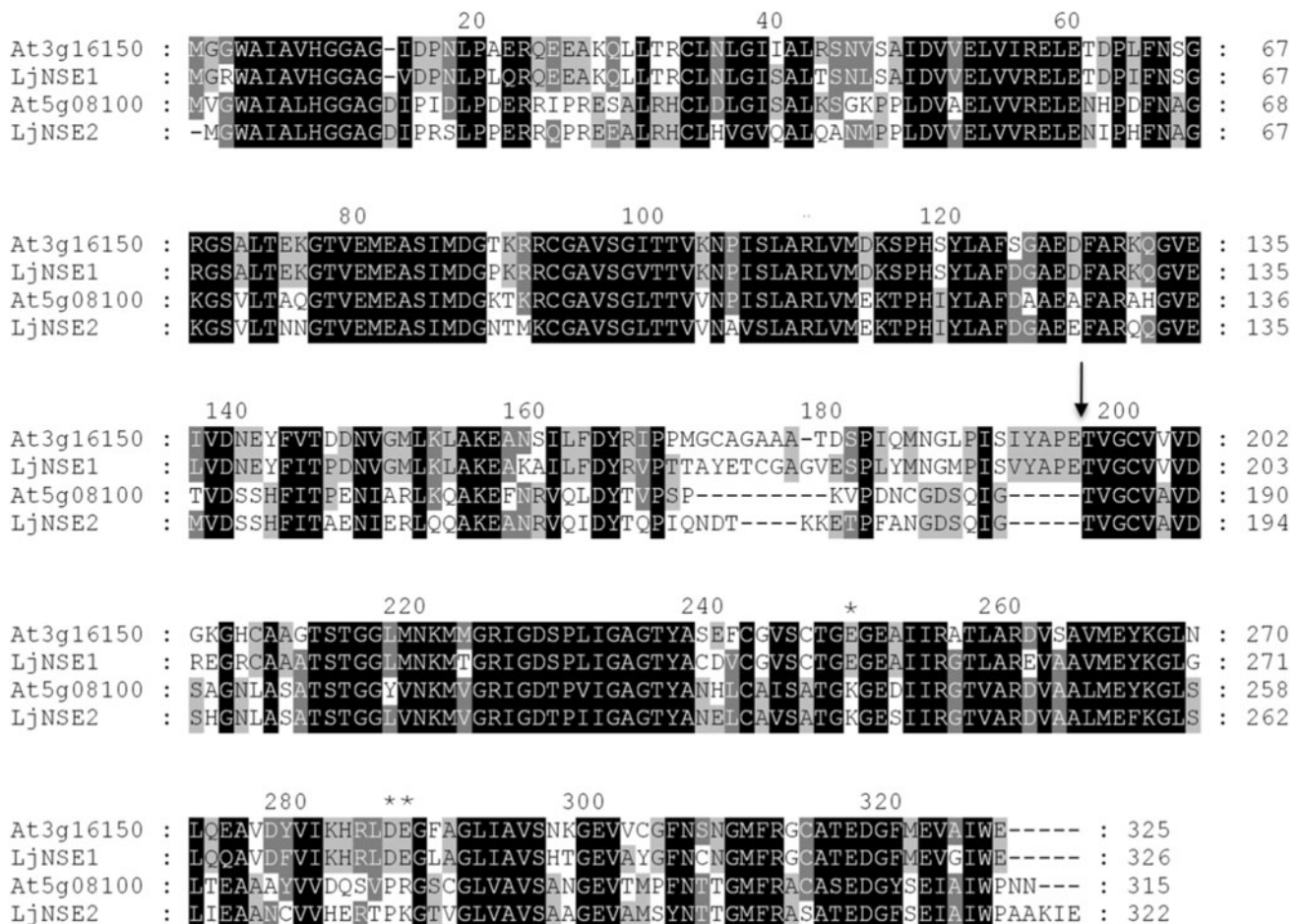


Fig. 1 Sequence alignment of asparaginases from *L. japonicus* and *A. thaliana*. The autoproteolytic cleavage site is indicated by an arrow. The alignment was generated using CLUSTALW (Thompson et al. 1994) at the European Bioinformatics Institute website and displayed with ESPript (Gouet et al. 1999) (accessed at <http://www.ca.expasy.org>). Gaps in the alignment are shown by black

dashes. Identical or similar residues conserved in the four sequences are shown in black. Identical or similar residues conserved in three of the sequences are shown in dark gray (white letters). Identical or similar residues conserved in two of the sequences are shown in light gray (black letters). Site-directed mutagenized residues analyzed in this work are indicated by stars

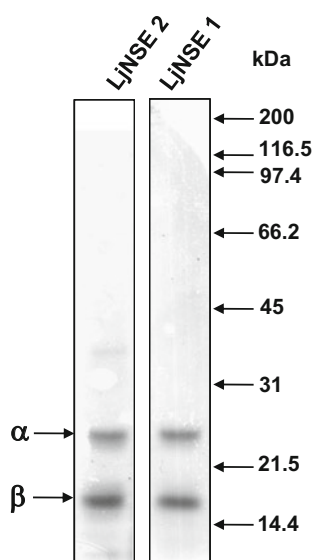


Fig. 2 SDS-PAGE of purified LjNSE1 and 2 asparaginases. Molecular mass (kDa) of standard proteins are indicated by *arrows*, as well as α and β subunits of asparaginase

catalytically active (T196 for LjNSE1 and T187 for LjNSE2) (Fig. 1).

Analytical ultracentrifugation of purified native asparaginases produced in *E. coli* established a sedimentation coefficient of 4.4 S, in each case, consistent with a frictional ratio of 1.4 for both isoenzymes and a native size of around 75–76 kDa (data not shown), which corresponds to the protein with poly His-tag whereas the theoretical molecular mass without the poly His-tag is around 70 kDa. These results are compatible with the characteristic $(\alpha\beta)_2$ quaternary structure of plant-type asparaginases.

Effect of K^+ on *L. japonicus* asparaginases enzyme activities

Figure 3a shows the asparaginase activity of LjNSE1 and LjNSE2, in the absence or presence of 50 mM K^+ in the assay mixture. Although the basal levels of LjNSE1 and LjNSE2 enzyme activities were very similar in the absence of K^+ , the activity of LjNSE1 was about ten times stimulated by the presence of 50 mM K^+ . In contrast, the activity of LjNSE2 was not significantly affected by K^+ , thus confirming that LjNSE1 and LjNSE2 represent a K^+ -dependent and K^+ -independent asparaginase isoforms, respectively, as presumed from previous protein sequence analysis. The kinetic response of LjNSE1 towards different K^+ concentrations gave a hyperbolic Michaelis–Menten behavior with a K_m for K^+ of 0.26 ± 0.03 mM (Fig. 3b). In order to determine the specificity for K^+ of LjNSE1, the effect of distinct monovalent and divalent cation was examined. K^+ produced the highest stimulation of LjNSE1 enzymatic activity, compared to Na^+ or Rb^+ . Other M^+ ,

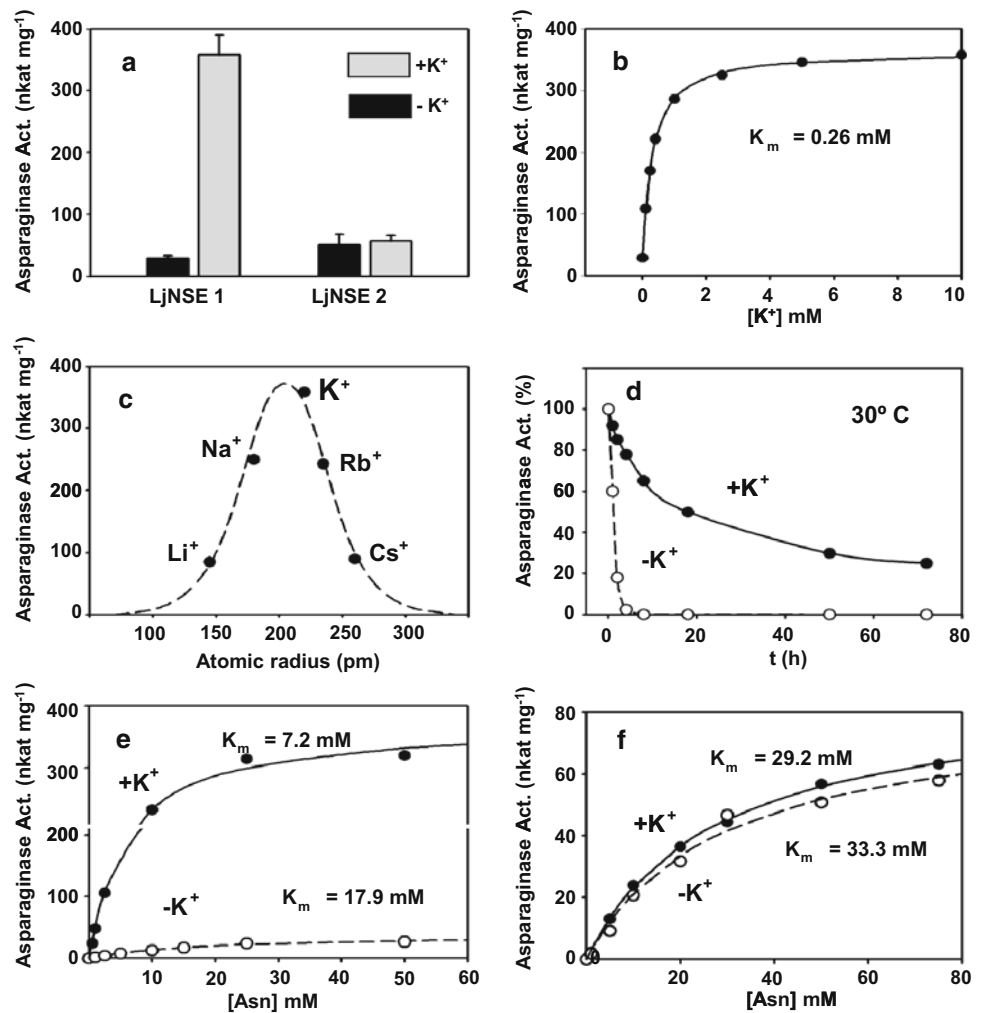
like Li^+ or Cs^+ , had only a minor effect on the activity (Fig. 3c). Thus, an interesting bell-shaped correlation between the M^+ atomic radius and asparaginase enzyme activity was observed, with an optimum for K^+ . The presence of divalent cation, like Ca^{2+} or Mg^{2+} , in the assay mixture did not produce any increase in LjNSE1 asparaginase enzyme activity (not shown), indicating that they cannot substitute for the effect of M^+ . In addition, it was also observed that the stimulating effect of M^+ was not affected by the counterion used (Cl^- , SO_4^{2-}). Likewise, the K^+ -dependent isoform, LjNSE1, was more thermostable in the presence of K^+ . While the half-life of the recombinant purified enzyme was 2 h after incubation at 30°C, in the absence of K^+ , this value increased up to 18 h by the presence of 50 mM K^+ (Fig. 3d).

Recombinant LjNSE1 showed a K_m for Asn of about 7.2 ± 1.67 mM in the presence of 50 mM K^+ , and 17.9 ± 0.45 mM in its absence. Hence, K^+ increases the affinity of the LjNSE1 enzyme for Asn (Fig. 3e). On the other hand, LjNSE2 showed a K_m for Asn around 30 mM, which did not change significantly by the presence of 50 mM K^+ in the assay mixture (29.2 ± 2.2 mM in the presence of 50 mM K^+ and 33.3 ± 6.7 mM in its absence) (Fig. 3f). It is important to note that His-tag and the additional peptide in the recombinant asparaginases do not affect the enzymatic activity. All these results clearly indicate that K^+ has an important significance for both asparaginase catalytic activity and the stability of LjNSE1 enzyme. In addition, it was also shown that LjNSE2 enzyme had β -aspartyl-hydrolase activity ($K_m = 0.54$ mM for β -Asp-His; Fig. S2 in Supplemental data). By contrast, no β -aspartyl-hydrolase activity was detected in the case of LjNSE1 isoform either in the presence or in the absence of K^+ .

Structure and function relations of K^+ -dependent asparaginase

Structural models for LjNSE1 and LjNSE2 isoenzymes were generated by simulated annealing. For this purpose, the geometrical restraints from the three-dimensional structure of close homologues were obtained (see “Materials and methods”). The template with the highest homology was the K^+ -independent asparaginase from *Lupinus luteus* (Michalska et al. 2006), which shows 56% of identity with the *L. japonicus* LjNSE1. The overall backbone RMSD of the different structures resulting from computations was 3.8 and 3.6 Å of LjNSE1 and 2, respectively. However, these values are low (0.98 and 0.34 Å, respectively) when excluding the non-conserved sequence stretch (residues 168–194 in LjNSE1). For further computations on LjNSE1, a representative subset of the structures, with a RMSD value of 2.24 Å for all backbone atoms, was selected and averaged.

Fig. 3 Effect of K^+ and other monovalent cations on the LjNSE1 and 2 enzyme activities. **a** Activity of the purified recombinant LjNSE preparations were measured in the absence or presence of 50 mM K^+ . **b** LjNSE1 asparaginase activity at different K^+ concentrations. **c** Correlation between cation atomic radius and the efficiency on the LjNSE1 activity stimulation. Enzyme activity was determined in the presence of 50 mM of the indicated cation. **d** A purified preparation of recombinant asparaginase was incubated at 30°C, in the presence (closed circles) or absence (open circles) of 50 mM K^+ . At the indicated times, the asparaginase activity was measured using an aliquot of the incubation mixtures. **e, f** Asparaginase activity at different Asn concentrations. The asparaginase activity was measured for LjNSE1 and 2 purified preparations in the absence (open circles) or presence (closed circles) of 50 mM K^+ , at the indicated Asn concentrations. Error bar SD



The molecular structures of LjNSE1 and 2 were created from four polypeptide chains. The biological assembly is therefore a heterotetramer ($\alpha\beta$)₂. The protein core is formed by two β -sheets, positioned in a face-to-face manner, with their strands following the same general direction. To assess the quality of the LjNSE1 model, this structure was compared to those of the templates. Overall, omitting the sequence stretch from 168 to 194, for which no previous structural data were available, the model backbone atoms showed a low RMSD (1.28 Å) with respect to those from the *Lupinus* template (Fig. 4a). Given that experimental data clearly indicates that no fragment is removed from the processed protein, we kept this variable loop in our models, using the average of the ensemble (5.3 Å RMSD for this loop) obtained by simulated annealing. The lack of a single structure in this loop is due to the absence of appropriate templates or to the high mobility in this region, leading to a small number of restraints to aid the computations.

The initial model consisted of a single $\alpha\beta$ precursor, and it was modified in silico to generate the resulting $\alpha\beta$

heterodimer. The dimer of heterodimers ($\alpha\beta$)₂ (Fig. 4b) was generated by structural alignment with the co-ordinates of plant K^+ -independent asparaginase (PDB code, 2GEZ). Thus, each $\alpha\beta$ heterodimer of the template was fit with the closest snapshot to the average structure from a molecular dynamics (MD) computation on the LjNSE1 $\alpha\beta$. In all the initial models, the active centre (Fig. 4c) shows the same features as those from bacterial asparaginases (Michalska et al. 2005, 2008), excepting the sugar-binding site, which is occupied by the side chain of E195—the C terminus residue of the first $\alpha\beta$ monomer after cleavage—it could explain the reduced reactivity of plant asparaginases towards glycosylated asparagine.

For comparative purposes, a model of the K^+ -independent homologous LjNSE2 was generated using the same templates. The cores of the two proteins were identical, since the RMSD of backbone co-ordinates of conserved residues (277 in total) is lower than 1 Å. Again, major differences were found in the region spanning from residue 150–185. However, the only significant difference as

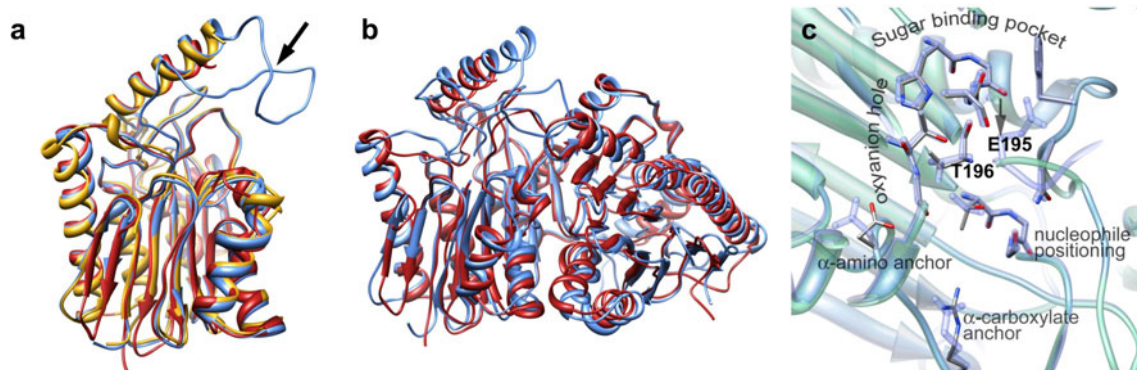


Fig. 4 Molecular modelling. **a** Overlay of the structures of α - β heterodimers from LjNSE1 (blue), *Lupinus* asparaginase (red, 2GEZ) and *E. coli* asparaginase (yellow, 2ZAK). The black arrow shows the variable loop. **b** Overlay of the tetrameric structure of LjNSE1 (blue)

regards the canonical active site (Fig. 4c) is the presence of E195 in LjNSE1, which is glycine (G186) in LjNSE2. This corresponds to the end of the variable loop, which does not appear in the template X-ray structures, and in both proteins blocks the access to the “sugar-binding” pocket, but not to the catalytic threonine (T196 and T187 in LjNSE1 and LjNSE2, respectively) residue.

Figure 5a shows a structural alignment to compare the two LjNSE1 and LjNSE2 models and map identical residues. As expected, the two β -sheets at the core of the protein are highly conserved. Opposite, two large low-identity regions were found. The first corresponds to residues 16–35 (loop 1 α -helix 1 in the α subunit), whose structure is conserved. The second low-identity stretch spans from residues 158–195 in LjNSE1, corresponding to the variable loop in the model. Helix 1 is rich in ionic residues in both proteins, but they show a different distribution and net charge. In fact, the K^+ -independent enzyme LjNSE2 is richer in basic residues. Hence, although the electrostatic surface potentials (ESP) of the two proteins are similar, some particular areas show substantial differences (Fig. 5b, c). Specifically, the ESP of LjNSE1 shows some negative patches that are absent in LjNSE2. The most significant one (black arrow in Fig. 5b) corresponds to charge replacements that take place at the rim of the active site crevice. E248 at loop 4 (linking α -strand 4 and α -helix 1) of the β subunit of LjNSE1 is a lysine (K239) in LjNSE2. Moreover, nearby D285 and E286, which locate in loop 6 between α -helix 3 and β -strand 5 of the β monomer in LjNSE1, are replaced by proline (P276) and lysine (K277), respectively, in LjNSE2. A second negative patch locates at a cavity behind the active site, near a Na^+ binding site, conserved in all asparaginases (Michalska and Jaskolski 2006; Michalska et al. 2006), and involves, among others, D15 and the side chain of E195. This is due to the above-mentioned changes in loop 1 and helix 1 of the α subunit.

and plant asparaginase template (2GEZ). **c** Focus on the active site. Residues are oriented as in Fig. 9 from Michalska and Jaskolski (2006). Labels are adapted from the same source

Molecular dynamics of K^+ -interaction in LjNSE1

To test the effect of monovalent cations, the charge of the LjNSE1 $\alpha\beta$ heterodimer model was neutralized in five distinct simulations with Li^+ , Na^+ , K^+ , Rb^+ and Cs^+ , respectively, and solvated (Fig. 6a). Taking into account the periodic cell volume (see Table S1 in Supplemental data) the ion concentration in these simulations were ca. 370 mM. It is worth mentioning that ions were allocated according to the coulombic potential around the protein. In all cases, a monovalent cation was placed near E286 in LjNSE1, which is K277 in LjNSE2. Notably, this ion was the only one keeping its initial position along the first ns of MD, in case of the heterodimer. In the tetramer model, one K^+ ion was similarly placed beside each of the two active centres. Along the MD, one of the K^+ remained longer at the same position (Fig. 6b), whereas the other one showed a larger mobility from the beginning (Fig. 6c).

The overall results of MD computations on the different models are shown in Fig. 7. In all cases the core of the structure remained unchanged, but the all-residues backbone RMSDs (Fig. 7, left) drifted significantly in the trajectories wherein Li^+ or Cs^+ had been added instead of Na^+ , K^+ , or Rb^+ , in agreement with the experimental data. Noteworthy, the variable region in the α -monomer remains anchored to the core by its C terminus, which was generated by in silico cleavage of the precursor monomer to generate the $\alpha\beta$ heterodimer. In fact, the radius of gyration of the protein is 19.0 ± 0.1 Å along all simulations. Moreover, despite being the region with largest atomic fluctuations, they remain moderate in the presence of Na^+ , K^+ or Rb^+ , but not in the presence of Li^+ or Cs^+ (Fig. 7, right). A remarkable overall correlation was found between the experimentally determined activity of the enzyme and average fluctuations of residues 181–195 (Fig. 7, right, insert) at the C terminus of the α subunit. Notably, this region is highly conserved in K^+ -dependent plant enzymes

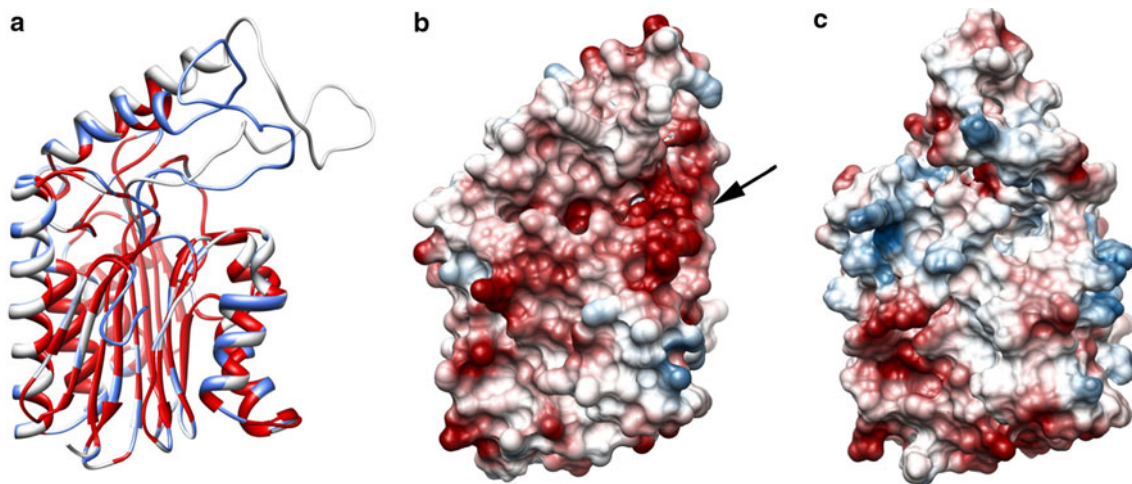


Fig. 5 **a** Overlay of the homology models of LjNSE1 and LjNSE2 heterodimers. Heterodimers are oriented with their interaction surfaces pointing to the right. Identical residues are highlighted in *red*, those not conserved are in *white* (LjNSE1) or *cyan* (LjNSE2). **b, c** Electrostatic potentials (*red* negative, *blue* positive) at the surface

of LjNSE1 (**b**) and LjNSE2 (**c**) heterodimers, as calculated using Coulomb equations and a distance-dependent dielectric constant. The two protein structures were aligned for these representations. *Arrow* in **b** points to enhanced negative patch near the active site which is further analyzed in this work

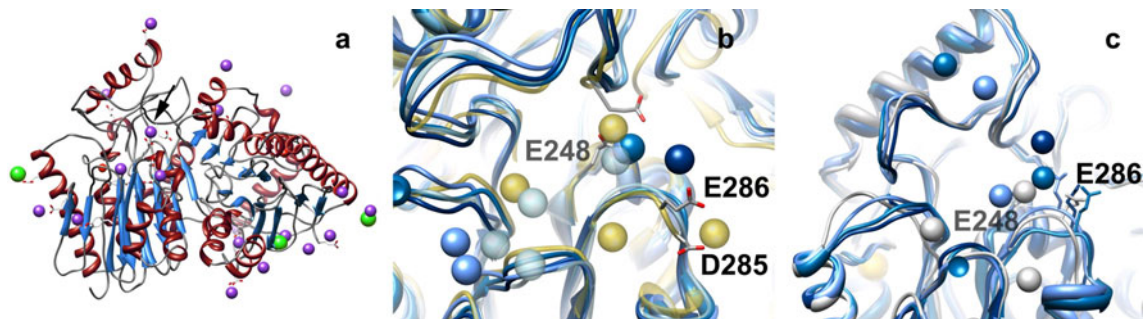


Fig. 6 Location of monovalent ions in LjNSE1. **a** Model structure (TLEAP output) of LjNSE1 tetramers used as input in MD computations. K^+ is in *purple*, Cl^- is in *green*, Na^+ is in *red*. Na^+ ions were allocated according to the position of this ion in template coordinates, by structural alignment. Cl^- and K^+ coordinates were set by search of hotspots in the electrostatic grid, as implemented in TLEAP. *Arrow* points out K^+ ion further analyzed in **b**. **b** K^+ ions near the open active site along the first 800 ps of MD computations on

the LjNSE1 tetramer. K^+ ions and the protein ribbon are colored according to the snapshot time: energy minimized structure is in *yellow*, 0 ps in *white*, 400 ps in *cyan*, 600 ps in *blue*, 800 ps in *dark blue*. Side chains from acidic residues at distances shorter than 5 Å are represented in *sticks*. Acidic residues conserved in K^+ -dependent asparaginases are labeled. **c** K^+ ions near the second (closing) active site along the first 800 ps of MD computations on the LjNSE1 tetramer, colored as in **b**

but not in the K^+ -independent ones, to which all XRD structures reported correspond.

The energy minimized average structure of the MD trajectory of the $\alpha\beta$ heterodimer in the presence of K^+ was used to build the whole enzyme tetramer and submitted again to MD computations in the presence of either K^+ or Li^+ together with the sodium, calcium and chloride ions near the protein in the template coordinates. The atomic fluctuations along simulations behaved as for isolated $\alpha\beta$ heterodimers in the presence of K^+ , but it was observed that one heterodimer showed larger fluctuations no matter K^+ or Li^+ was present. In this particular heterodimer, K^+ left its original position near E286 at the beginning of computations (see below). We tested then whether the two

active sites were accessible to the substrate, selecting the coordinate set from the trajectory with lower RMSD with respect to the average. Notably, only one of the active sites is clearly accessible in the presence of K^+ , a small pocket of 712 Å³ volume, 615 Å² surface and 143 Å² of mouth surface (Fig. S3 in Supplemental data). Remarkably, MD calculation reflected that K^+ near this site (Fig. 6b) binds more tightly than the equivalent near the other active site (Fig. 6c) which remained unavailable. None of the two sites were open in the presence of Li^+ . To further test if the active site cavity could accommodate the substrate, we performed a series of docking computations of Asn into LjNSE1 (Fig. 8). The structure of LjNSE1 from simulations in the presence of K^+ lodges Asn within the active

Fig. 7 Molecular dynamics calculations of LjNSE1 heterodimers. *Left* RMSD of backbone coordinates along the MD trajectories with respect to the initial energy minimized structures. *Right* RMSF calculated along the trajectories. *Insert* Correlation between atomic fluctuations of the sequence stretch containing residues 180–195 and the specific activity of the enzyme

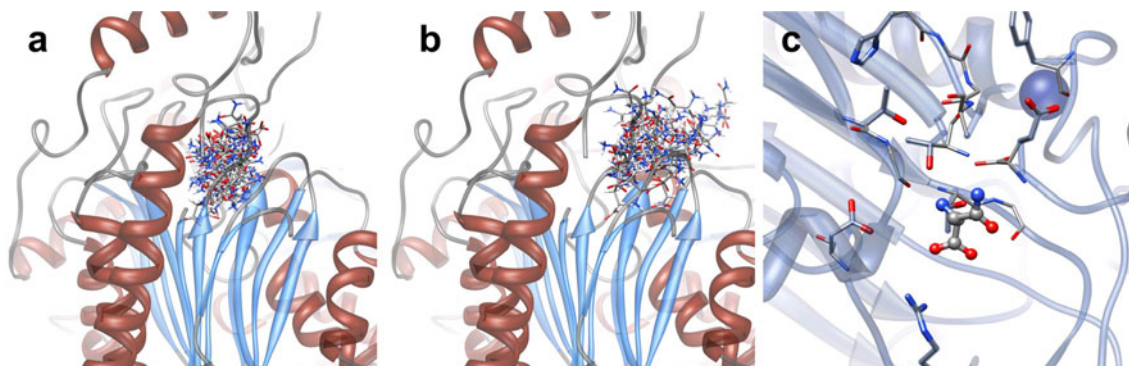
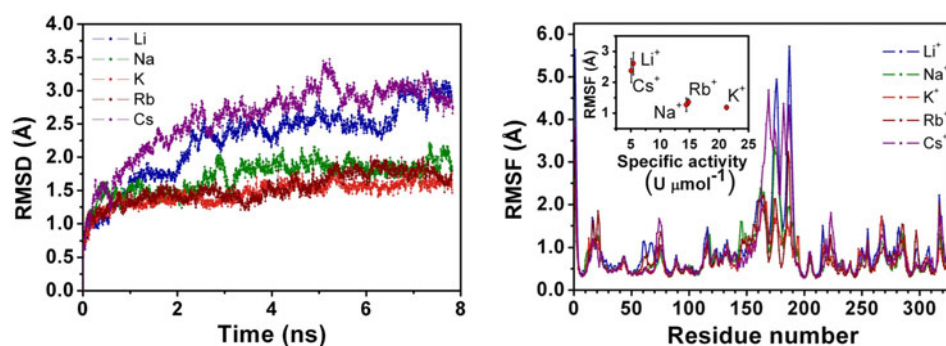


Fig. 8 Docking computations of Asn into LjNSE1. **a** Structure with K^+ : 50 best scored structures: LjNSE1 is represented as *ribbon*, Asn molecules as *sticks*. **b** Structure with Li^+ : 50 best scored structures. **c** Active site: Asn is in *ball* and *sticks*, active site side chains are

represented in *sticks*. The *blue sphere* corresponds to a Na^+ ion conserved in all asparaginases structures, which was included in all calculations

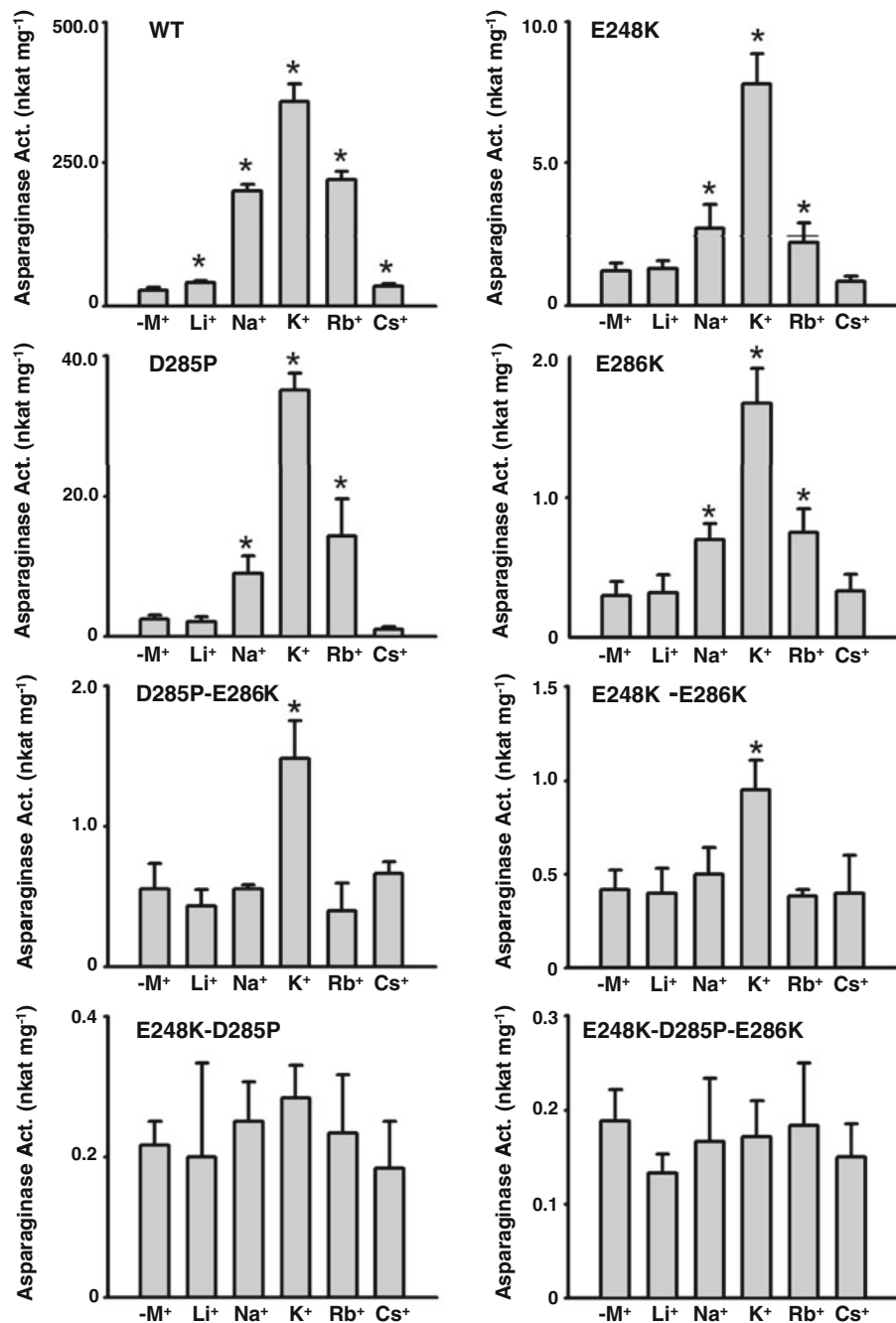
site (Fig. 8a, c), but the substrate amino acid remains outside, far from the catalytic threonine (T196), when the Li^+ structure is employed in the computations (Fig. 8b).

Site-directed mutagenesis of asparaginase residues involved in K^+ interaction

Previous results emphasize the presence of a crevice near the negatively charged loop region comprising residues E248, D285 and E286, in the β subunit, from the core and located at the mouth of the active site pocket (Fig. 6b), as the most likely candidates for the interaction of the LjNSE1 protein with K^+ (M^+). A site-directed mutagenesis approach was used to target these negatively charged amino acid residues present in LjNSE1 enzyme, replacing them by the corresponding residues present in K^+ -independent LjNSE2 isoform (E248K, D285P and E286K substitutions, respectively). Single-site mutant enzymes affected on each of these residues were tested for their asparaginase activity in the presence or absence of 50 mM of different monovalent metal cation (Cs^+ , Li^+ , Rb^+ , Na^+ , K^+) (Fig. 9). Enzyme activity was substantially lowered on each of the mutant; however, all of them kept the K^+ -activity activation property. In the case of D285P mutant the asparaginase activity was affected in the same

proportion in the presence or absence of K^+ and, consequently, the $+K^+/-M^+$ enzyme activity ratio remained practically unaffected (Fig. 4, in the Supplementary material). This ratio was reduced by half in the case of E248K and E286K mutants since K^+ -dependent enzyme activity was lowered to a higher extent compared to the enzyme activity in the absence of M^+ . Based on the previous results, a set of double mutants and a triple mutant was produced to determine if K^+ dependence of LjNSE1 enzyme activity could disappear as a result of targeting two or three of the acidic residues located on this region at the same time. The obtained data presented in Fig. 9 shows that only the activity of the E248K-D285P double mutant and the E248K-D285P-E286K triple mutant lost the K^+ -activation sensitivity, thus indicating that the examined residues, particularly E248 and E286, are crucial for K^+ requirement of LjNSE1 enzyme, thus offering intriguing clues to their possible role in K^+ coordination. Interestingly, Fig. 9 also shows that mutant enzymes in the aforementioned residues had lower asparaginase activation by other M^+ , particularly Cs^+ and Li^+ , when compared to the behavior of the WT form. In addition to D285, E286 and E248 residues, other negatively charged residues from LjNSE1, absent in LjNSE2, have been also mutated (D15 and E179, at the α subunit, and E195, at the active site just

Fig. 9 Effect of M^+ on the activity of purified LjNSE1 from wild type and mutants. Asparaginase activity was determined, as indicated in “Materials and methods”, using as enzyme source the wild type or the indicated single, double or triple LjNSE1 mutants obtained by site-directed mutagenesis, and including in the assay mixture 50 mM of the indicated cation. Error bar SD. Activity values significantly different from the activity levels without M^+ are marked with an asterisk ($P \leq 0.05$ Student’s *t* test)



next to catalytic T196) but the dependence for K^+ of LjNSE1 asparaginase activity could not be suppressed (results not shown).

Discussion

In this work, a K^+ -dependent (LjNSE1) and K^+ -independent (LjNSE2) asparaginase isoforms from the model legume *L. japonicus* have been comparatively analyzed. Sequence identity profiles (Fig. 1) are consistent with the

genealogic tree of Bruneau et al. (2006) for plant asparaginases, where K^+ -dependent and K^+ -independent activity enzymes were separated very early in the evolution.

Plant asparaginases have been purified from different plant species (Lea et al. 2007). The reported Asn K_m values of asparaginases purified from plants range over 3–12 mM approx. 100-fold higher than those of most animal and bacterial enzymes (Chang and Farnden 1981). Bacterial-type asparaginase has been used as a therapeutic agent against acute lymphoblastic leukemia (Verma et al. 2007). Asparaginase from *Withania somnifera* is the first plant-type

enzyme probed to be effective as therapeutic agent (Oza et al. 2010), but the K_m for Asn is 0.06 mM (Oza et al. 2009), which is very low, as compared with the K_m of other plant-type enzymes.

Recombinant asparaginases from *L. japonicus* also showed high Asn K_m values, in the range described for most plant enzymes. Nevertheless, it was found that Asn K_m values were considerably lower for the K^+ -dependent LjNSE1 isoform, compared to K^+ -independent LjNSE2 (Fig. 3). The presence of K^+ in the enzyme reaction assay further increased the affinity of LjNSE1 enzyme for Asn, at the same time than activity value for this enzyme was highly stimulated by K^+ being tenfold more active than the corresponding K^+ -independent LjNSE2 isoform. In addition, the LjNSE1 enzyme was shown to be also stabilized by K^+ . The existence of an asparaginase isoform with a higher enzyme activity and higher affinity for Asn must be of crucial importance for plants that use Asn as a N transport compound, such as *L. japonicus*, and suggests that LjNSE1 must be the main enzyme responsible for the utilization of Asn in this plant, in accordance with the highest level of expression of this particular isoform in sink tissues of the plant (data not shown).

The high K_m value for Asn observed for LjNSE2 (around 30 mM) suggests that this particular isoenzyme may have a physiological role unrelated to the hydrolysis of Asn in vivo, particularly because the Asn concentration in xylem sap from *L. japonicus* is in the range of 6–17 mM (Waterhouse et al. 1996). However, LjNSE2 enzyme shows an efficient β -aspartyl-hydrolase activity ($K_m = 0.54 \pm 0.02$ mM for β -Asp-His), while this was not the case for the K^+ -dependent isoform LjNSE1. Catalytic efficiency of LjNSE2 isoform is 12-fold higher with β -Asp-His hydrolase than asparaginase activity. As various isoaspartyl peptides are known to arise from proteolytic degradation of post-translationally altered proteins containing isoaspartyl residues, plant-type asparaginases may not only function in Asn catabolism but also as detoxifying enzymes (Bruneau et al. 2006). According to this proposal, K^+ -independent activity LjNSE2 is probably a detoxifying enzyme in *L. japonicus*.

Numerous enzymes in plants are activated by monovalent cation (M^+) (Page and Di Cera 2006). The role of M^+ on enzyme activation is to facilitate substrate binding by lowering energy barriers in the ground and/or transition states rather than being a causative agent of catalysis. The inability of M^+ to be directly involved in the catalysis, unlike the metal divalent cation does, is usually due to insufficient charge density resulting to spread a single charge over a large volume. Enzymes exhibiting a cofactor-like response to K^+ activation are termed type I (Page and Di Cera 2006). They are absolutely dependent upon M^+ , which is required either for substrate binding (type Ia) or for substrate hydrolysis (type Ib). Enzymes exhibiting an allosteric response to K^+ are categorized as type II (Page

and Di Cera 2006). In this case, although their activity is not absolutely dependent on M^+ , it is enhanced through protein conformational changes triggered by M^+ interaction and not involving direct contact with the substrate. According to these data, LjNSE1 is a type II Ntn-hydrolase enzyme with respect to K^+ .

In this paper we have analyzed in deep the molecular features responsible for K^+ dependence of plant asparaginase proteins, for which no structure–function studies were available. In the absence of a crystal structure for a K^+ -dependent asparaginase, homology modelling and molecular dynamics were used in this work to state a model for tertiary and quaternary structure of the $(\alpha\beta)_2$ heterotetramer, revealing key features of the structure and function of *L. japonicus* asparaginases. Homology modelling has been recently used to identify key amino acids involved in the potassium binding region in an apple terpene synthase (Green et al. 2009). In the present work we identified a region within LjNSE1 from *L. japonicus* that exhibited potential for K^+ -binding. This led to the identification of the “surface-exposed holes” in LjNSE1 comprising negatively charged amino acid residues E248, D285 and E286. It is frequent that metal binding sites in proteins are formed by small loops in the polypeptide that provide a set of 3–4 ligands and thus define the site (Williams 1998). K^+ -dependent LjNSE1 asparaginase appears to be another of such examples where the above-mentioned ligands must contribute to the coordination of K^+ .

Site-directed mutagenesis combined with structural and kinetic studies gave an almost complete picture of the K^+ -enzyme interaction. We propose that E248, D285 and E286 are the key amino acid residues for K^+ coordination and thus for asparaginase activity stimulation. When considering that six ligands in octahedral configuration is the most commonly observed geometry for M^+ coordination (Page and Di Cera 2006) it is likely that at least one and possibly two water molecules will prove to be involved in the completion of the K^+ coordination in the LjNSE1 from *L. japonicus* and may be in other K^+ -dependent plant asparaginases.

Acknowledgments Supported by Junta de Andalucía (Grants BIO-163, BIO-198 and P07-CVI-3026) and Spanish Ministerio de Ciencia e Innovación (Grant BFU2009-07190). We are indebted to R. Rodríguez for assistance in MALDI experiments, G. Estivill in figures performance, and P. Díaz and G. Quero for ANOVA tests. We also thank M. J. Cubas for technical assistance.

References

- Aitken A (2005) Identification of protein by MALDI-TOF MS. In: Walker J (ed) Proteomics protocol handbook. Humana Press, Totowa, pp 319–324

- Bendsten JD, Nielsen H, Heijne GH, Brunak S (2004) Improved prediction of signal peptides: SignalP 3.0. *J Mol Biol* 340: 783–795
- Berendsen HJC, Postma JPM, Vangunsteren WF, Dinola A, Haak JR (1984) Molecular-dynamics with coupling to an external bath. *J Chem Phys* 81:3684–3690
- Berman HM, Westbrook J, Feng Z, Gilliland G, Bhat TN, Weissig H, Shindyalov IN, Bourne PE (2000) The protein data bank. *Nucleic Acids Res* 28:235–242
- Borek D, Jaskolski M (2001) Sequence analysis of enzymes with asparaginase activity. *Acta Biochim Pol* 48:893–902
- Borek D, Michalska K, Brzeczinski K, Kisiel A, Podkowinski J, Bonthron DT, Krowarsch D, Otlewski J, Jaskolski M (2004) Expression, purification and catalytic activity of *Lupinus luteus* asparagine β -amidohydrolase and its *Escherichia coli* homolog. *Eur J Biochem* 271:3215–3226
- Bradford MM (1976) A rapid and sensitive method for quantitation of microgram quantities of protein utilizing the principle of protein-dye binding. *Anal Biochem* 72:248–254
- Bruneau L, Chapman R, Marsolais F (2006) Co-occurrence of both L-asparaginase subtypes in *Arabidopsis*: At3g16150 encodes a K⁺-dependent L-asparaginase. *Planta* 224:668–679
- Cañas RA, de la Torre F, Cánovas FM, Cantón FR (2007) Coordination of PsAS1 and PsASPG expression controls timing of re-allocated N utilization in hypocotyls of pine seedlings. *Planta* 225:1205–1219
- Case DA, Darden TA, Cheatham TE III, Simmerling CL, Wang J, Duke RE, Luo R, Merz KM, Pearlman DA, Crowley M, Walker RC, Zhang W, Wang B, Hayyik S, Roitberg A, Seabra G, Wong KF, Paesani F, Wu X, Brozell S, Tsui V, Gohlke H, Yang L, Tan C, Mongan J, Hornak V, Cui G, Beroza P, Matthews DH, Schafmeister C, Ross WS, Kollman PA (2006) AMBER, 9th edn. University of California, San Francisco
- Chang KS, Farnden KJF (1981) Purification and properties of asparaginase from *Lupinus arboreus* and *Lupinus angustifolius*. *Arch Biochem Biophys* 208:49–58
- Dundas J, Ouyang Z, Tseng J, Binkowski A, Turpaz Y, Liang J (2006) CASTp: computed atlas of surface topography of proteins with structural and topographical mapping of functionally annotated residues. *Nucleic Acid Res* 34 (Web Server issue): W116–W118
- Eswar N, Eramian D, Webb B, Shen M-Y, Sali A (2008) Protein structure modelling with MODELLER. *Methods Mol Biol* 426:145–159
- Gouet P, Courcelle E, Stuart DI, Métoz F (1999) ESPript: analysis of multiple sequence alignment in PostScript. *Bioinformatics* 15:305–308
- Green S, Squire CJ, Nieuwenhuizen NJ, Baker EN, Laing W (2009) Defining the potassium binding region in an apple terpene synthase. *J Biol Chem* 284:8661–8669
- Handberg K, Stougaard J (1992) *Lotus japonicus*, an autogamous, diploid legume species for classical and molecular genetics. *Plant J* 2:487–496
- Humphrey W, Dalke A, Schulten K (1996) VMD: visual molecular dynamics. *J Mol Graphics* 14:33–38
- Jorgensen WL, Chandrasekhar J, Madura JD, Impey RW, Klein ML (1983) Comparison of simple potential functions for simulating liquid water. *J Chem Phys* 79:926–935
- Kabsch W, Sander C (1983) Dictionary of protein secondary structure: pattern recognition of hydrogen-bonded and geometrical features. *Biopolymers* 12:2577–2637
- Laemmli UK (1970) Cleavage of structural protein during the assembly of the head of bacteriophage T4. *Nature* 227:680–685
- Lang PT, Brozell SR, Mukherjee S, Pettersen ET, Meng EC, Thomas V, Rizzo RC, Case DA, James TL, Kuntz ID (2009) DOCK 6: combining techniques to model RNA-small molecules complexes. *RNA* 15:1219–1230
- Laue TM, Shall BD, Ridgeway TM, Pelletier SL (1992) Computer-aided interpretation of analytical sedimentation data for proteins. In: Harding SE, Rowe AJ, Horton JC (eds) Analytical ultracentrifugation in biochemistry and polymer science. The Royal Society of Chemistry, Cambridge, pp 90–125
- Lea PJ, Sodek L, Parry MAJ, Shewry PR, Halford NG (2007) Asparagine in plants. *Ann Appl Biol* 150:1–26
- Leigh RA, Wyn Jones RG (1984) A hypothesis relating critical potassium concentrations for growth to the distribution and functions of this ion in the plant cell. *New Phytol* 97:1–13
- Márquez AJ (2005) *Lotus japonicus* handbook. Springer, Dordrecht
- Márquez AJ, Betti M, García-Calderón M, Pal'ove-Balang P, Díaz P, Monza J (2005) Nitrate assimilation in *Lotus japonicus*. *J Exp Bot* 56:1741–1749
- Marschner H (1995) Mineral nutrition of higher plants, 2nd edn. Academic Press, London
- Michalska K, Jaskolski M (2006) Structural aspects of L-asparaginases, their friends and relations. *Acta Biochim Pol* 53:627–640
- Michalska K, Brzezinski K, Jaskolski M (2005) Crystal structure of isoaspartylaminopeptidase in complex with L-aspartate. *J Biol Chem* 280:28484–28491
- Michalska K, Bujacz G, Jaskolski M (2006) Crystal structure of plant asparaginase. *J Mol Biol* 360:105–116
- Michalska K, Hernández-Santoyo A, Jaskolski M (2008) The mechanism of autocatalytic activation of plant-type L-asparaginases. *J Biol Chem* 283:13388–13397
- Möllering H (1985) L-aspartate and L-asparagine. In: Bergmeyer HU, Bergmeyer J, Grass IM (eds) Methods of enzymatic analysis, vol VIII, 3rd edn. VCH Verlagsgesellschaft, Weinheim, pp 350–357
- Nielsen H, Engelbrech J, Brunak S, Heijne G (1997) Identification of prokaryotic and eukaryotic signal peptides and prediction of their cleavage sites. *Protein Eng* 10:1–6
- Oza VP, Trivedi SD, Parmar PP, Subramanian RB (2009) *Withania somnifera* (ashwagandha): a novel source of L-asparaginase. *J Integrative Plant Biol* 51:201–206
- Oza VP, Parmar PP, Kumar S, Subramanian RB (2010) Anticancer properties of highly purified L-asparaginase from *Withania somnifera* L. against acute lymphoblastic leukemia. *Appl Biochem Biotechnol* 160:1833–1840
- Page MJ, Di Cera E (2006) Role of Na⁺ and K⁺ in enzyme function. *Physiol Rev* 86:1049–1092
- Pettersen EFG, Huang CC, Couch GS, Greenblatt DM, Meng EC, Ferrin TE (2004) UCSF Chimera—a visualization system for exploratory research and analysis. *J Comput Chem* 25:1605–1612
- Philo JS (1997) An improved function for fitting sedimentation velocity data for low molecular-weight solutes. *Biophys J* 72:435–444
- Ryckaert JP, Ciccoli G, Berendsen HJC (1977) Numerical integration of the Cartesian equations of motion of a system with constraints: molecular dynamics of n-alkanes. *J Comput Phys* 23:327–341
- Sodek L, Lea PJ, Mifflin BJ (1980) Distribution and properties of a potassium-dependent asparaginase isolated from developing seeds of *Pisum sativum* and other plants. *Plant Physiol* 65:22–26
- Stacey G, Libault M, Brechenmacher L, Wan J, May GD (2006) Genetics and functional genomics of legume nodulation. *Curr Opin Plant Biol* 9:110–121
- Thompson JD, Higgins DG, Gibson TJ (1994) CLUSTAL W: improving the sensitivity of progressive multiple sequence alignment through sequence weighting, position-specific gap penalties and weight matrix choice. *Nucleic Acids Res* 22:4673–4680
- Udvardi MK, Tabata S, Parniske M, Stougaard J (2005) *Lotus japonicus*: legume research in the fast line. *Trends Plant Sci* 10:222–228

- Verma N, Kumar K, Kaur G, Anand S (2007) L-Asparaginase: a promising chemotherapeutic agent. *Crit Rev Biotechnol* 27:45–62
- Wang JM, Cieplak P, Kollman PA (2000) How well does a restrained electrostatic potential (RESP) model perform in calculating conformational energies of organic and biological molecules? *J Comput Chem* 21:1049–1074
- Waterhouse RN, Smyth AJ, Massonneau A, Prosser IM, Clarkson DT (1996) Molecular cloning and characterisation of asparagine synthetase from *Lotus japonicus*: dynamics of asparagine synthesis in N-sufficient conditions. *Plant Mol Biol* 30:883–897
- Williams NH (1998) Phosphate diesterases and triesterases. In: Sinnott M (ed) *Comprehensive biological catalysis*, vol 1. Reaction of electrophilic carbon, phosphorus and sulfur. Academic Press, London, pp 543–557